A NONLINEAR MODEL PREDICTIVE CONTROL ALGORITHM FOR BREAST CANCER TREATMENT

Jeffry A. Florian, Jr. [*] **Julie L. Eiseman** [**,***]
Robert S. Parker [*,***,1]

[*] *Department of Chemical and Petroleum Engineering, University of Pittsburgh School of Engineering, Pittsburgh, PA*
[**] *Department of Pharmacology, University of Pittsburgh School of Medicine, Pittsburgh, PA*
[***] *Molecular Therapeutics and Drug Discovery Program, University of Pittsburgh Cancer Institute, Pittsburgh, PA*

Abstract: A nonlinear model predictive control (NMPC) algorithm was developed to dose the chemotherapeutic tamoxifen to mice bearing breast cancer xenografts. A novel saturating rate cell-cycle model (SCM) was developed to capture unperturbed tumor growth dynamics, and a bilinear tumor kill term was included in the G-phase to account for the cycle-specific nature of tamoxifen and its active metabolite. Drug pharmacokinetics were modeled using a three-compartment linear model, which successfully approximated parent compound and metabolite (4-hydroxytamoxifen) plasma concentrations as a function of time. Using daily tumor measurements, the model predictive control algorithm successfully reduced tumor volume along a specified reference trajectory over a period of 4 months. A more clinically-relevant implementation using weekly or biweekly tumor measurements, and a prediction horizon seven days beyond the measurement interval, also led to reduced tumor volumes. In the mismatch case, a controller based on the simpler linear cell-cycle model (LCM) was unable to track desired reductions in tumor volume. Controllers based on a lumped-parameter saturating Gompertz model (GM), however, can yield similar performance to those using the more complex saturating rate cell-cycle model. This performance was dependent on the cell-cycle phase of drug effect, with poorer results for M-phase targeted drugs. Overall, NMPC is a suitable algorithm for the class of chemotherapy problems with daily drug dosing, and the algorithm developed here may be adaptable to the clinical setting for the treatment of human breast cancer patients.

Keywords: biomedical systems, nonlinear models, nonlinear model predictive control

1. INTRODUCTION

Cancer is the second-leading cause of death in the United States and is responsible for $189.5 billion in health care and research costs (The American Cancer Society, 2004). It is estimated that more than 1.4 million new cancer cases will be diagnosed in the year 2004 alone (The American Cancer Society, 2004). Given the economic and societal impact of the disease, improved treatment algorithms could lead to dramatic reductions in morbidity and economic burden by increasing treatment efficacy and efficiency. Mathematical models of untreated or treated tumor growth have been developed with varying levels of complexity from the cellular to the macroscopic scale (Norton, 1988; Asachenkov *et al.*, 1994; Bajzer *et al.*, 1996). Furthermore, the medical community focuses significant energy on

[1] To whom correspondence should be addressed: rparker@pitt.edu; +1-412-624-7364; 1249 Benedum Hall, Pittsburgh, PA 15261 USA

the development of mathematical models of drug pharmacokinetics using available tools (D'Argenio and Schumitzky, 1997). Using case study specific models, the cancer chemotherapy treatment problem can be posed in a model-based framework.

In fact, for more than a decade, various model-based cancer treatment algorithms have been synthesized with a focus on batch-like problems (Martin, 1992; Panetta and Adam, 1995; Harrold *et al.*, 2003). The main focus of these approaches is to calculate a treatment profile over a fixed duration that satisfies a performance objective including, among other terms, minimizing tumor size at a specified future time. The durations may be as short as a cycle of therapy (28 days in (Harrold *et al.*, 2003)) or as long as a full course of therapy (52 weeks or more in (Martin, 1992)). The latter is a generic optimal treatment problem using a "drug" and "tumor" with assumed dynamic behavior; these problems can be solved using a variety of methods including control vector parameterization (Martin and Teo, 1994) and optimal control theory (Ledzewicz and Schättler, 2002). However, clinically-unrealistic assumptions about the efficacy of compounds or treatment modalities (such as continuous infusion over *days*) limit the impact of generic formulations. To improve the potential significance, case-study specific information from human or animal studies, which includes tumor growth, drug effect, toxicity, etc., are incorporated into the mathematical models of pharmacokinetics (PK) and pharmacodynamics (PD). Given these models, one can pose cyclical cancer treatment as a mixed-integer optimization problem (Harrold *et al.*, 2003).

Not all cancer treatment problems have the pseudo-batch structure outlined above. One such example, and the case study evaluated in this work, is the treatment of estrogen receptor positive (ER+) breast cancer xenografts by the chemotherapeutic tamoxifen (TM). The parent compound and its more active metabolite 4-hydroxytamoxifen (HTM) function through competitive inhibition with estrogen. Drug-binding prevents receptor activation and causes an accumulation of cells in late G_1 phase due to growth signal truncation. While neither the parent nor active metabolite directly induce cell apoptosis (programmed cell death), the cell stress resulting from accumulation causes increased apoptosis as a function of the total tumor size and the amount of drug administered. TM treatment is the method of choice against ER+ breast cancer, not only due to its effectiveness but also because of its low toxicity that enables long term dosing with minimal side effects (Ellis and Swain, 2001). A typical TM regimen might involve the patient taking daily TM doses for up to 5 years. Hence, it should be possible to develop a NMPC algorithm to dose breast cancer patients with TM. The present work addresses the synthesis of this algorithm in the context of a preclinical mouse study using mice bearing human breast cancer xenografts.

2. METHODS

Pharmacokinetic data were obtained from Robinson *et al.* (1991). A single large dose of TM (200 $\frac{\text{mg}}{\text{kg}}$) was administered orally (in 0.1 mL peanut oil) to non-tumor-bearing, ovariectomized, athymic mice, and plasma samples were taken at 0, 3, 6, 12, 24, 48, 72, and 96 hours after dosing. Plasma samples were purified using chromatography; concentrations of TM, HTM, and N-desmethyltamoxifen were determined via comparison to a standard curve and the resulting plasma concentrations represent the averaged values from three mice.

Tumor volume data for pharmacodynamic modeling were obtained from Conley and coauthors (1999). The study protocol involved athymic mice implanted subcutaneously with ER+ xenografts and estradiol pellets at day 0. Stratified groups were dosed via oral gavage at 7.5, 15, 30, of 60 $\frac{\text{mg}}{\text{kg}}$ tamoxifen per day dissolved in 0.1 mL of purified water (vehicle had no significant effect on tumor growth). Doses were given once a day for five consecutive days followed by two days off, beginning on day 12 of the study. This seven-day pattern was repeated twice. Twice each week, tumor volumes were recorded using digital calipers assuming an ellipsoidal tumor of volume $\frac{\ell w^2}{2}$ (ℓ = longest tumor axis, w = shortest tumor axis perpendicular to ℓ).

In this paper, different models with similar names and structures are presented. Tables 1 and 2 provide a summary of the model abbreviations employed throughout.

3. TUMOR GROWTH MODELING

Common models for describing untreated tumor growth include the exponential and Gompertz, among others (Martin and Teo, 1994). Biologically motivated

Table 1. Open-loop model nomenclature

SCM	saturating rate cell-cycle model (unperturbed)
SCM-G	saturating rate cell-cycle model with G-phase kill
SCM-M	saturating rate cell-cycle model with M-phase kill
GM	Gompertz model (with kill term)
LCM	linear cell-cycle model
LCM-G	linear cell-cycle model with G-phase kill

Table 2. Closed-loop model nomenclature

NC-G	nominal case; controller designed using SCM-G
NC-M	nominal case; controller designed using SCM-M
MC-Gu	mismatch case; SCM-G as the simulated mouse; controller designed using GM at equivalent input to SCM-G
MC-Mu	mismatch case; SCM-M as the simulated mouse; controller designed using GM at equivalent input to SCM-M
MC-My	mismatch case; SCM-M as the simulated mouse; controller designed using GM at equivalent output to SCM-M

cell-cycle models provide more insight into cell behavior (Panetta and Adam, 1995), but these linear state space models display exponential growth and are unable to capture saturating tumor growth dynamics. The Gompertz model (GM) is capable of capturing clinically observed tumor dynamics (Norton, 1988), but it does not capture information regarding the progression of cells through the individual phases of the cell-cycle. Cell cycle information is vital from a treatment perspective because cycle-specific anti-cancer compounds such as curacin A, Taxol, and tamoxifen can be modeled in a biologically meaningful manner (Lopes *et al.*, 1993; Panetta and Adam, 1995; Kozusko *et al.*, 2001). To accurately model both declining tumor growth rate and cell phase distribution, a saturating rate cell-cycle model (SCM) was constructed (Florian Jr. *et al.*, 2003):

$$\frac{dX_G}{dt} = -k_G X_G \ln\left(\frac{\theta}{N}\right) + 2k_M X_M \ln\left(\frac{\theta}{N}\right) \quad (1)$$

$$\frac{dX_S}{dt} = -k_S X_S + k_G X_G \ln\left(\frac{\theta}{N}\right) \quad (2)$$

$$\frac{dX_M}{dt} = -k_M X_M \ln\left(\frac{\theta}{N}\right) + k_S X_S \quad (3)$$

$$N = X_G + X_S + X_M \quad (4)$$

Here X_i corresponds to the volume (mm^3) of cells (assuming constant cell volume and 10^6 cells = 1 mm^3) in the G (growing), S (DNA synthesis), or M (mitosis) phases; θ is the plateau population of the tumor ($10^5\,mm^3$); and k_i's denote transfer rates between cell phases ($\frac{1}{hr}$). The three states correspond to cells in G_0/G_1 (G), S, or G_2/M (M) phases, and groupings were selected based on experimental limitations. Representations of the five-compartment cell-cycle model and the reduced three-compartment cell-cycle model are shown in Figure 1. Flow cytometry separates cells based on total DNA content and a fluorescent DNA label, such as propodium iodine (Lee *et al.*, 2002). Cell phases possessing equivalent amounts of DNA emit the same fluorescence. The G_0 and G_1 phases contain the same amount of DNA, hence they are indistinguishable and are lumped together into the single phase, G. The same scenario applies for cells in the G_2 and M phases, which contain twice the DNA as the cell prepares to divide (Riesberg *et al.*, 2001).

Two alternative tumor growth models, the three compartment linear cell-cycle model (LCM) and the GM were simulated for comparison with the above model. Removing the logarithmic total population dependence from individual transition rates in Equations (1)-(3) results in the following governing equations for the LCM:

$$\frac{dX_G}{dt} = -k_G X_G + 2k_M X_M \quad (5)$$

$$\frac{dX_S}{dt} = -k_S X_S + k_G X_G \quad (6)$$

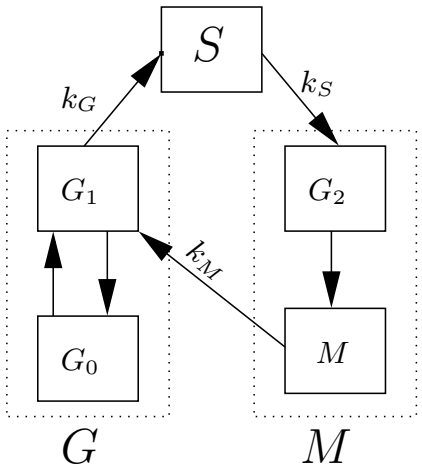

Fig. 1. The five phases of the cell-cycle: G_0 (senescence), G_1 (growth), S (DNA replication), G_2 (mitotic preparation), and M (mitosis). Evaluating fractional distributions via fluorescent DNA labeling and flow cytometry prevents unique quantification of G_0 from G_1 (lumped as G) and G_2 from M (lumped as M).

$$\frac{dX_M}{dt} = -k_M X_M + k_S X_S \quad (7)$$

$$N = X_G + X_S + X_M \quad (8)$$

The Gompertz model lumps cell phases into one homogeneous population, N, with saturating growth dynamics as $N \to \theta$:

$$\frac{dN}{dt} = \tau N \ln\left(\frac{\theta}{N}\right) \quad (9)$$

All constants and variables are equivalent to previous definitions; τ is a pseudo-doubling time ($\frac{1}{hr}$).

Values for the transfer rates (k_i) and the pseudo-doubling time (τ) were determined by minimizing the squared difference between model predictions and animal data (Conley *et al.*, 1999). The model parameters are summarized in Table 3. The tumor data and model predictions are plotted in Figure 2. Both the SCM and GM provide an accurate prediction of tumor growth over the duration of the experiment. In contrast, the LCM is unable to account for both rapid initial tumor proliferation and the decreasing growth rate observed with increasing tumor size. Rather, it predicts an average fit of the growth data.

Table 3. Parameter values for the tumor growth models: linear cell-cycle (LCM), Gompertz (GM), and saturating rate cell-cycle (SCM).

	LCM	GM	SCM
k_g	0.0168	—	0.0013
k_s	0.0088	—	0.0390
k_M	0.0429	—	0.0169
τ	—	.0010	—
θ	—	10^5	10^5

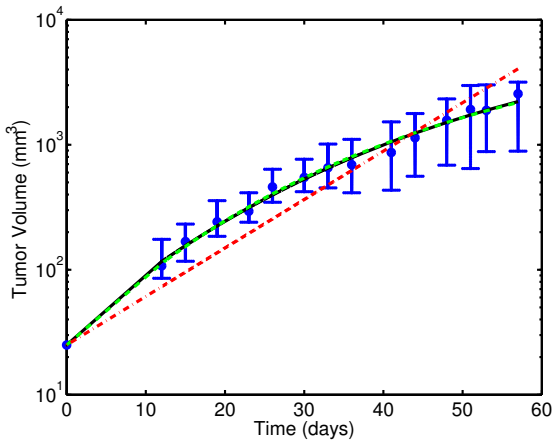

Fig. 2. Measured mean tumor volume data (circles; N = 20 control mice) and simulated tumor size (lines) as a function of time for LCM (dash-dot), SCM (solid), and GM (dash, overlay on solid) models. Error bars represent a 95% confidence interval.

Akaikie's Information Criteria, traditionally used by the medical community to assess whether increases in model complexity are justified by improvements in model accuracy, is given by (Akaike, 1979):

$$\mathrm{AIC} = n \ln\left(\frac{\mathrm{SSE}}{n}\right) + 2 * p \tag{10}$$

Here, SSE is the sum squared error between the model prediction and the data at the measurement points, n is the number of data points, and p is the number of parameters in the model. Since the number of data points (17) and the SSE for both models were equivalent (13.98 for each) while the number of parameters increased from 1 to 3, AIC analysis clearly favored the simpler Gompertz description. However, this result was not unexpected and should result if the SCM accurately portrays Gompertz growth while maintaining cell phase information. The benefit of including additional complexity in this case allowed for an accurately targeted drug-effect when a cycle-specific chemotherapeutic was employed. It was anticipated that this improvement in model quality will lead to improved performance by controllers designed from this model (Morari and Zafiriou, 1989).

4. PHARMACOKINETICS

The pharmacokinetics of the oral agent TM and its active metabolite HTM were modeled using the first-order parent/metabolite with oral dosing compartmental structure in Figure 3. A TM dose is administered orally, and the parent compound is absorbed from the gut. After absorption, circulating TM can be cleared from the system (including conversion to metabolites such as tamoxifen N-oxide, N-desmethyltamoxifen, and others) or converted to HTM. Circulating HTM is also cleared from the

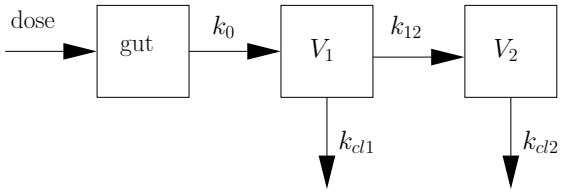

Fig. 3. 3-compartment model for plasma concentrations of tamoxifen and 4-hydroxytamoxifen after oral dosing

system. Of the metabolites, only HTM and N-desmethyltamoxifen appear in plasma at detectable concentrations (Ellis and Swain, 2001). Affinity studies have shown N-desmethyltamoxifen binds with estrogen receptors at $\frac{1}{50}$ the affinity of TM and $\frac{1}{1250}$ the affinity of HTM (Ellis and Swain, 2001). As such, only TM and HTM are postulated to contribute a significant anti-tumor effect.

The following equations describe the TM and HTM pharmacokinetics:

$$\begin{aligned}
\frac{dX_0}{dt} &= -k_0 X_0 + u(t) \\
\frac{dX_1}{dt} &= -k_{cl1} X_1 - k_{12} X_1 + k_0 X_0 \\
\frac{dX_2}{dt} &= -k_{cl2} X_2 + k_{12} X_1 \\
Y_1 &= \frac{X_1}{V_1} \\
Y_2 &= \frac{X_2}{V_2}
\end{aligned} \tag{11}$$

Here X_0, X_1, and X_2 correspond to TM mass in the gut, TM mass in plasma, and HTM mass in plasma, respectively (μg), V_1 and V_2 are central compartment volumes for the parent compound and metabolite (mL), and k_i denote transfer rates ($\frac{1}{\mathrm{hr}}$). Variables Y_1 and Y_2 represent the measured plasma concentrations of TM and HTM ($\frac{\mu\mathrm{g}}{\mathrm{mL}}$).

The parameters in equations (11) were fit by minimizing the squared difference between model predictions and data obtained from non-tumor bearing athymic mice (Robinson *et al.*, 1991) and the resulting parameter values are summarized in Table 4.

Model predictions for both compounds can be seen in Figure 4. The pharmacokinetic model is able to capture the dynamic profile of the data with only a slight over-prediction of TM concentration

Table 4. PK parameter values for the oral dosing of tamoxifen.

Parameter	Value
k_0	0.052 $\frac{1}{\mathrm{hr}}$
k_{12}	0.340 $\frac{1}{\mathrm{hr}}$
k_{cl1}	0.349 $\frac{1}{\mathrm{hr}}$
k_{cl2}	14.866 $\frac{1}{\mathrm{hr}}$
V_1	2.354 mL
V_2	0.060 mL

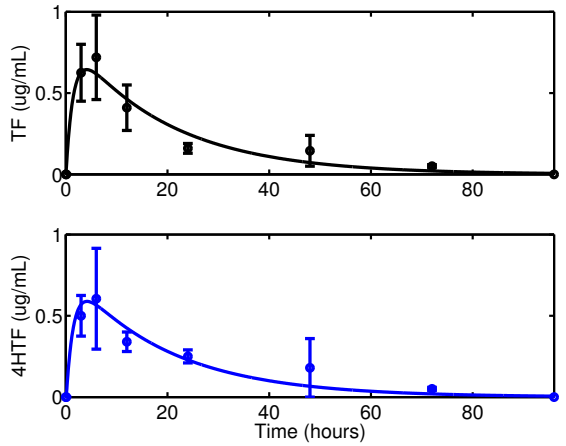

Fig. 4. Actual (circles) vs. simulated (lines) PK for TM (top) and HTM (bottom) after a 200 mg/kg oral dose of TM. Each data point represents mean plasma concentrations from three mice; error bars are $\pm$ 1 standard deviation.

at $t = 24$ hours. Additional compartments or delays could be incorporated into the TM model to more accurately fit the data at the cost of increased number of parameters, decreased parameter confidence, and increased mathematical complexity.

5. PHARMACODYNAMICS

The cycle-specific drug effects of TM and HTM were coupled with the tumor growth model by including a bilinear kill term in the differential equation for X_G in (1), termed the saturating rate cell-cycle model with G-phase kill (SCM-G). Cycle-specific drug effects were also incorporated for X_G in (5) and for N in (9), respectively. Conceptually, the bilinear structure means that increases in drug concentration have an increasing anti-tumor effect and a larger tumor will have more cells susceptible to a given dose. Adding the bilinear term yields the following modifications to equations (1), (5), and (9), respectively:

$$\frac{dX_G}{dt} = -k_G X_G \ln\left(\frac{\theta}{N}\right) + 2k_M X_M \ln\left(\frac{\theta}{N}\right) - k_D X_G \left(\frac{X_1}{V_1} + c\frac{X_2}{V_2}\right) \quad (12)$$

$$\frac{dX_G}{dt} = -k_G X_G + 2k_M X_M - k_D X_G \left(\frac{X_1}{V_1} + c\frac{X_2}{V_2}\right) \quad (13)$$

$$\frac{dN}{dt} = \tau N \ln\left(\frac{\theta}{N}\right) - k_D X_G \left(\frac{X_1}{V_1} + c\frac{X_2}{V_2}\right) \quad (14)$$

Here k_D is the drug-induced tumor death rate ($\frac{\text{mL}}{\mu\text{g hr}}$) and c represents the ratio between the binding affinities of TM and HTM. Combining the kill rates in this manner is justified based on the inhibition mechanism of the drug, which involves the blockage of estrogen receptor sites. A drug which binds more tightly to the receptor acts as a more potent blocker, and the relative strength of that bond serves as a basis of comparison for its effectiveness versus other drugs. As noted above, HTM has been shown experimentally to possess a binding affinity 25-50 times that of TM (Ellis and Swain, 2001), so c was set to 25 (possibly underestimating HTM anti-tumor effect).

Unperturbed tumor growth rates and PK parameters were fixed at identified values, and k_D was estimated by minimizing the squared difference between the data and SCM-G predictions at each of four dosing levels (60, 30, 15, and 7.5 $\frac{\text{mg}}{\text{kg}}$ per dose). The k_D rates corresponding to the three lower dosing levels were found to be in close agreement ($0.00251 \pm 0.00025 \frac{\text{mL}}{\mu\text{g hr}}$), while the rate for 60 $\frac{\text{mg}}{\text{kg}}$ was significantly lower ($0.00192 \frac{\text{mL}}{\mu\text{g hr}}$). This discrepancy is possibly due to a saturation of the estrogen receptor pathway at the high dose level. By limiting the dosing levels to $0 \le u(t) \le 30 \frac{\text{mg}}{\text{kg}}$ per day (single daily dose), the value of k_D can be fixed to the mean value of $0.00251 \frac{\text{mL}}{\mu\text{g hr}}$. Although Conley *et al.* (1999) did not demonstrate long term survival of mice on daily TM dosing, other authors have shown mouse longevity for up to 2 years at $40 \frac{\text{mg}}{\text{kg}}$ daily dosing, thereby validating the dosing range used here as within acceptable toxicity limits (Martin *et al.*, 1997).

Estimating k_D for both the LCM-G and GM yielded similar rate trends for k_D. At the three lower dosing levels ($30, 15$, and $7.5 \frac{\text{mg}}{\text{kg}}$), k_D values were in close agreement (LCM-G: $0.00531 \pm 0.00047 \frac{\text{mL}}{\mu\text{g hr}}$; GM: $0.00325 \pm 0.00024 \frac{\text{mL}}{\mu\text{g hr}}$) while rates at $60 \frac{\text{mg}}{\text{kg}}$ (LCM-G: $0.00384 \frac{\text{mL}}{\mu\text{g hr}}$; GM: $0.00192 \frac{\text{mL}}{\mu\text{g hr}}$) were quite different. Estimated k_D rates between the GM and SCM-G were also similar while rates determined for the LCM-G were quite different. It is likely this change results from the linear vs. nonlinear dynamic structure of the models.

Figure 5 shows the ability of the pharmacodynamic models to fit tumor growth during treatment (dose $\le 30 \frac{\text{mg}}{\text{kg}}$). The model over-predicts drug effect for doses of 15 and 30 $\frac{\text{mg}}{\text{kg}}$, however these over-predictions do not seriously impact overall tumor growth predictions over the 60 day period. A portion of this mismatch results from fixing the unperturbed tumor growth kinetics, which were different even among stratified groups. For example, at day twelve for $30 \frac{\text{mg}}{\text{kg}}$ dosing (Figure 5, bottom) the predicted tumor size is greater than the measured tumor size on day 12 before drug is administered. Still, the model predicts the qualitative shape of drug-altered tumor growth and model predictions remain within the 95% confidence intervals.

6. CONTROLLER SYNTHESIS: SATURATING RATE MODEL

A daily dose of 12.0 mg/kg TM applied to the "simulated mouse" having PK governed by Equation (11) and SCM-G pharmacodynamics given by Equations (12), (2), (3), and (4) resulted in a steady state xenograft tumor burden of 100 mm^3. Note that the term "steady state" describes a tumor volume measurement taken at the same time each day. The bolus administration of TM resulted in periodic drug and tumor volume profiles, but measurements taken at 24-hour intervals were steady. A nonlinear model predictive control (NMPC) algorithm was developed to regulate tumor volume (measured variable) by manipulating TM dose on a daily schedule. In the nominal case, this algorithm uses the previously developed PK model in equation (11) and the PD model from equations (2) to (4) and (12) to explicitly predict the future tumor size based on the current and past dosing profile. The delivery problem formulation facilitated using the "$\Delta\mathscr{U}$" structure for the NMPC problem. The standard two-norm squared control objective was employed (Morari and Ricker, 1994):

$$\min_{\Delta\mathscr{U}(k|k)} \|\Gamma_y\left[\mathscr{R}(k+1)-\mathscr{Y}(k+1|k)\right]\|_2^2 + \|\Gamma_u\Delta\mathscr{U}(k|k)\|_2^2 \qquad (15)$$

Here $\mathscr{Y}(k+1|k)$ is the predicted future tumor volume over the prediction horizon of length p, $\mathscr{R}(k+1)$ is the desired tumor volume over the same horizon, and $\Delta\mathscr{U}(k|k)$ is the (move horizon, m, length) trajectory of future TM dosing changes calculated to minimize the objective (15). The weighting matrices Γ_y and Γ_u establish the relative importance of setpoint tracking error and manipulated variable movement, respectively; in the present work, these were set to $\Gamma_y = 1$ and $\Gamma_u = 0$ for all simulations. Magnitude

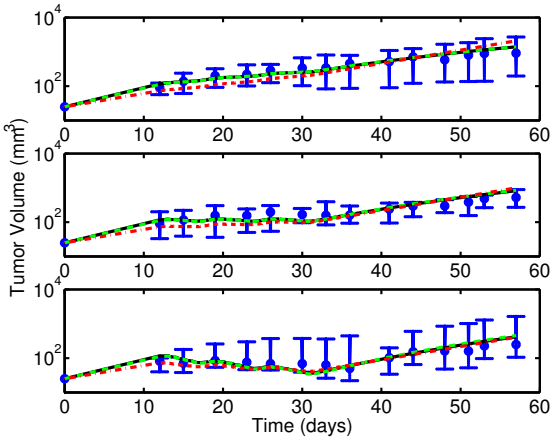

Fig. 5. Measured MCF-7 tumor xenograft data from tumor-bearing athymic mice (circles) vs. LCM-G (dash-dot), SCM-G (solid), and GM (dashed) model predictions at daily oral dose levels of 7.5 (top), 15 (middle) or 30 mg/kg (bottom) TM. Error bars represent a 95% confidence interval.

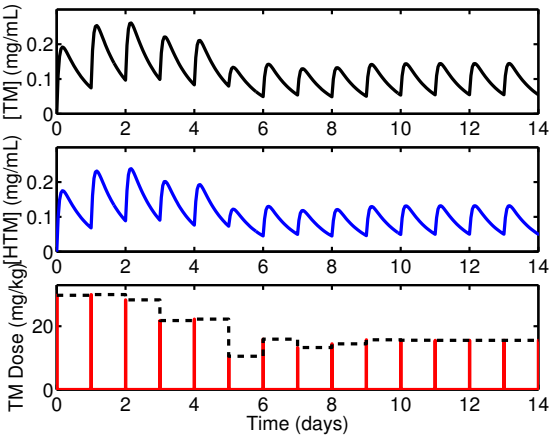

Fig. 6. TM plasma concentration (top), HTM plasma concentration (middle) and delivered TM oral dose (bottom) as a function of time. The dashed line in the bottom figure is the representation of NMPC results for easy viewing in longer simulations.

constraints were imposed to keep the daily TM dose within the bounds prescribed by the linearity in the PD effect with dose: $0 \le \mathscr{U}(k|k) \le 30\frac{\text{mg}}{\text{kg}}$. The resulting nonlinear programming problem was solved using the *fmincon* function in MATLAB (©2004, The MathWorks, Natick, MA). The studies evaluated in the remainder of this section are nominal control studies, with plant and model equivalent. The goal was to evaluate the performance of an NMPC controller formulation on a representative cancer chemotherapy problem.

Chemotherapy dosing differs from traditional engineering control systems in the manner of drug delivery. TM was delivered as a bolus each day by oral gavage in animal studies; this is conceptually similar to administering the chemotherapeutic as a pill. Hence, the "stepwise-constant" manipulated variable was replaced by a daily bolus. TM plasma concentration, HTM plasma concentration, and TM dose are shown in Figure 6. Each day a bolus was given (bottom, solid), and the corresponding TM (top) and HTM (middle) concentrations showed the characteristic rapid concentration rise and then decreasing plasma concentration over the course of the day. Of note is the accumulation of TM and HTM in the plasma; a pseudo-steady state was reached after about 10 days. The manipulated variable plot (bottom) in Figure 6 provides the actual dosing profile (solid) and this dose plotted in the traditional stepwise-constant shape (dashed). For ease of viewing in longer simulations, the stepwise-constant shape is plotted in future figures; *this stepwise shape is representative of the TM dose and is not the exact dosing profile*.

Controller tuning, *i.e.* setting the move and prediction horizons, is often accomplished on an *ad hoc* basis. Three candidate tuning sets for this case study are shown in Figure 7. The "simulated mouse" initially

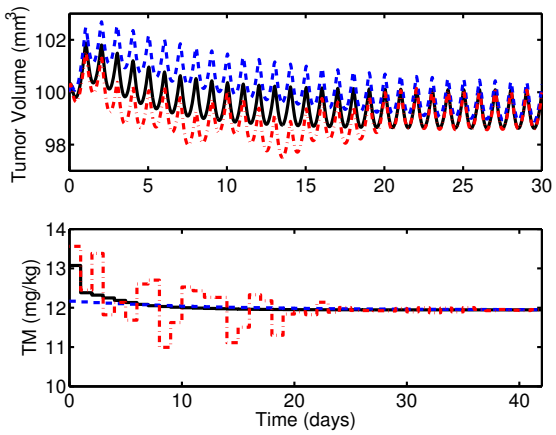

Fig. 7. Tumor volume (top) and TM dose representation (bottom) versus time for $m = 1$ with $p = 8$ (solid) and $p = 22$ (dashed) as well as $m = 2$, $p = 8$ (dash-dot).

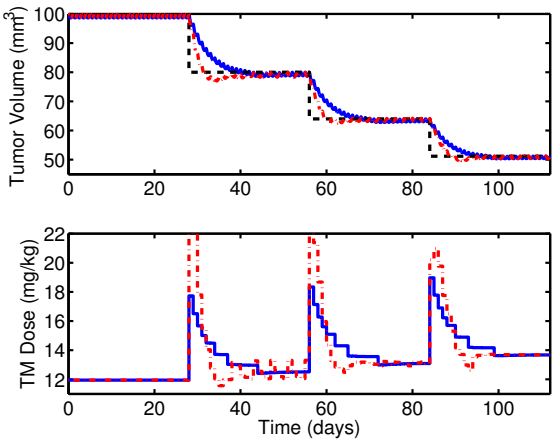

Fig. 8. Tumor volume (top), reference volume (dashed, top) and TM dose representation (bottom) as a function of time. Controller tunings are $m = 1$ (solid) and $m = 2$ (dash-dot) with $p = 8$.

had a 100 mm^3 tumor burden and TM and HTM plasma concentrations of 0; the NMPC controller was started with a reference value of 100 mm^3. Tumor measurements were taken at 24-hour intervals. All three tunings resulted in increased TM doses to offset the initial rise in tumor volume due to unperturbed tumor growth. As drug plasma concentrations rose over the first few days, tumor volumes started to decrease. After 56 days, the controller had achieved a pseudo-steady tumor burden of 100 mm^3. Settling to within 1% of the desired trajectory ($t_{99\%}$) for the $m = 1$, $p = 22$ case required markedly more time than the other two tests; this was rejected as a suitable controller tuning. From the bottom panel of Figure 7, the aggressiveness of the $m = 2$ controller can be observed; dose levels were changed about the mean value for approximately 3 weeks. The $m = 1$, $p = 8$ profile offered a smooth dosing profile and comparatively rapid return to the 100 mm^3 reference.

To determine which of the other two settings ($m = 1, p = 8$ or $m = 2, p = 8$) provided superior performance, a second trajectory was simulated. The ability of the different NMPC controller tunings to reduce tumor volume is shown in Figure 8. At four-week intervals (corresponding approximately to a "cycle" of traditional cancer chemotherapy), the tumor volume reference was decreased by 20% of the then-current value. The ability of the two controller tunings to track the reference changes from 100 to 80, 64, and 51.2 mm^3, respectively, was quite good. As expected, the more aggressive $m = 2$ tuning reduced tumor volume more quickly, but this led to increased undershoot with each step change and oscillatory dosing profiles. While the aggressive $m = 2$ trajectory reduced tumor size faster, the smoother $m = 1$ dosing profile is more acceptable from a clinical perspective.

An inherent assumption to this point is the ability to collect a tumor measurement on a daily basis. While this might be possible in animal studies at increased expense (using straightforward digital caliper measurements), the cost and impact on patient quality of life are prohibitive in human trials. The most frequent rate at which a tumor size measurement may be possible in humans is weekly without either the development of a new measurement technology or a reduction in time and cost associated with current measurements. In the nominal case, the following problem was posed. On day 0, and at 7-day (days 7, 14, etc.) or 14-day (days 14, 28, etc.) intervals, a tumor volume measurement was taken. The controller was formulated with $m = 1$ and $p = 14$ or $p = 21$ for weekly and biweekly measurement, respectively. The updated dose level calculated by the NMPC algorithm was delivered daily until the next measurement was obtained, and the controller computation was repeated. The results are shown in Figure 9. The weekly measurement had a $t_{99\%}$ value of 2 weeks, demonstrating excellent reference tracking performance. The slower measurement rate resulted in undershoot with a $t_{99\%}$ of 4 weeks which, as expected, was worse than the settling time from weekly updates. In the case that biweekly measurement is all that is available, the control algorithm can successfully reduce tumor volume.

7. CONTROLLER MODEL MISMATCH

The ability of the NMPC algorithm to perform despite mismatch between the actual and controller models was evaluated. The "simulated mouse" was taken as the actual system, and either the LCM-G or GM served as the controller model. As a tumor possesses a population of cells in different phases of the cell cycle and the overall growth dynamics saturate, these choices represent a fair depiction of overall tumor behavior. Furthermore, the robustness of developed control systems based on models failing to capture either nonlinear dynamic or cell-cycle information was assessed. Tracking tumor volume deviations with

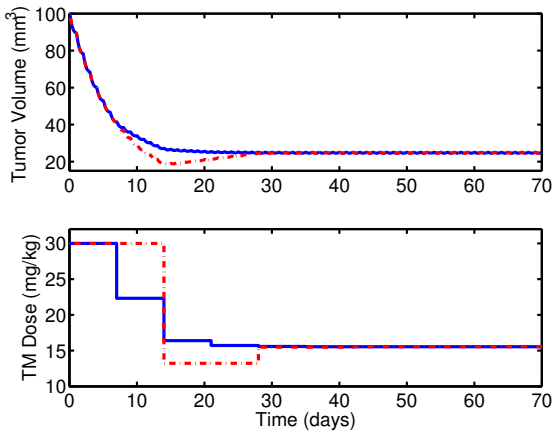

Fig. 9. Tumor volume (top) and TM dose representation (bottom) as a function of time. Tumor volumes are measured weekly (solid) or biweekly (dash-dot) under NMPC with $m = 1$, $p = 14$ (solid) or $p = 21$ (dash-dot). The tumor volume reference value is 25 mm^3.

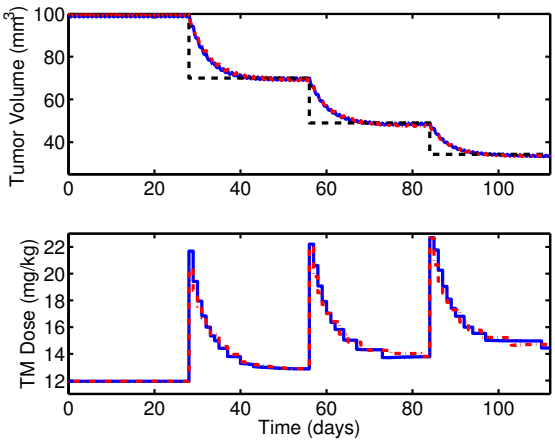

Fig. 10. Tumor volume (top), reference volume (dashed, top) and TM dose representation (bottom) as a function of time. Tuning parameters were chosen as m = 1 and p = 8 for both the nominal (NC-G, solid) and mismatch (MC-Gu, dash-dot) cases.

the LCM-G as the controller model was not possible, however, due to the differences in dynamic behavior between the LCM-G and SCM-G models over the dose range of interest. Further analysis with the linear cell-cycle model was discontinued as stability could not be guaranteed for progressive reductions in tumor volume.

Using the steady state input for the "simulated mouse" (12.0 $\frac{\text{mg}}{\text{kg day}}$ TM) resulted in a GM tumor burden of 104 mm^3. The controller model and the "simulated mouse" were initialized with the same steady state dose to allow manipulation of the daily dose over the full [0 $\frac{\text{mg}}{\text{kg}}$, 30 $\frac{\text{mg}}{\text{kg}}$] range. To assess controller performance under mismatch and to determine if the additional complexity of the SCM-G was necessary for high-performance control, closed-loop simulations were compared for two cases: a four-stage trajectory for tumor volume reduction with daily updates ($m = 1, p = 8$); and biweekly tumor volume updates ($m = 1; p = 21$) after a single reduction in desired tumor volume.

NMPC controller simulations for tracking stepwise tumor volume reductions under mismatched conditions employed desired tumor volume decrements of 30% between stages. This corresponded to reference trajectories of 100, 70, 51, and 34.3 mm^3 over each four-week cycle. The motivation for this alteration was to better utilize the allowable dosing range toward the maximum region (30 $\frac{\text{mg}}{\text{kg}}$); requiring greater tumor reduction during each step accomplished that task. The results are shown in Figure 10. The NMPC with the mismatched GM as the controller model initialized with the same input (MC-Gu) did not cause noticeable deviations from the nominal case with the SCM-G as the controller model (NC-G). The sum squared error increased by 10% (2603 vs. 2853 mm^6); this was primarily caused by the undershoot in the MC-Gu response profile. Differences in total drug delivered were negligible, though NC-G delivery profiles employed greater initial drug delivery in response to reference step changes. This resulted in a $t_{99\%}$ that was typically one day faster, occurring on day 14 (NC-G) vs. day 15 (MC-Gu) of each reference step. The MC-Gu also resulted in reference trajectory undershoot ranging from 1-2%. Both controllers led to tumor volumes that setttled to within 1% of the reference within the 4 weeks except the MC-Gu on the third stage (51 mm^3); 99% settling in the output occurred if the step was extended for longer than 28 days. Furthermore, the undershoot did not affect the ability of the MC-Gu to track the next tumor decrement.

Both controllers were also compared assuming tumor updates occurred every two weeks to better simulate clinical practice, and the results are shown in Figure 11. The input and output profiles were similar with reference deviation and total drug administered within 1% for the two systems. The $t_{99\%}$ settling time using the MC-Gu was markedly different, however, taking 111 days versus 29 for the NC-G.

Overall controller performance with the MC-Gu as the controller model did not differ significantly from controller performance using the NC-G, though the MC-Gu system displayed increased settling time in most cases. This agreement in performance was not unexpected. For the case of a G-phase-specific drug like TM, the SCM-G can be closely approximated as a Gompertz description at large tumor volumes. As the tumor size increases, a greater fraction of cells reside in G-phase; the SCM-G predicts 90% of the total cells in G-phase at a size of 100 mm^3 (increasing to 95% by 1000 mm^3). With the bulk of the population in G-

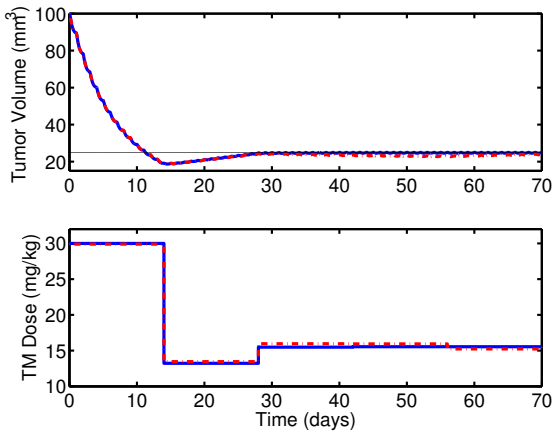

Fig. 11. Tumor volume (top) and TM dose representation (bottom) as a function of time. Tumor volumes are measured biweekly under NMPC with $m = 1$, $p = 21$ for the nominal (NC-G, solid) and mismatch (MC-Gu, dash-dot) cases. The tumor volume reference value is 25 mm^3.

phase along with the kill term, the dynamic behavior of the GM and SCM-G should be similar, as observed.

8. THEORETICAL STUDY: M-PHASE KILL

To test this hypothesis, a theoretical study was conducted using the same pharmacokinetic and pharmacodynamic data as the earlier studies within this paper. However, the PD effect was moved from the G-phase to the M-phase (where approximately 10% of the tumor cells reside), resulting in the following PD model (SCM-M):

$$\frac{dX_G}{dt} = -k_G X_G \ln\left(\frac{\theta}{N}\right) + 2k_M X_M \ln\left(\frac{\theta}{N}\right) \quad (16)$$

$$\frac{dX_S}{dt} = -k_S X_S + k_G X_G \ln\left(\frac{\theta}{N}\right)$$

$$\frac{dX_M}{dt} = -k_M X_M \ln\left(\frac{\theta}{N}\right) + k_S X_S - k_D X_G (X_1/V_1 + c X_2/V_2) \quad (17)$$

here equations (12) and (3) have been changed to equations (16) and (17), respectively, to reflect a drug acting primarily in the M-phase. The cell kill rate, k_D was determined as before for the four dosing levels (60, 30, 15, and 7.5 $\frac{\text{mg}}{\text{kg}}$). The rates for the three lower dosing levels were still in close agreement ($0.00161 \pm 0.00015 \frac{\text{mL}}{\mu\text{g hr}}$) while the kill rate corresponding to doses of 60 $\frac{\text{mg}}{\text{kg}}$ was again much lower (0.00090 $\frac{\text{mL}}{\mu\text{g hr}}$). This allowed the daily dosing range to be fixed as before, ($0 \le u(t) \le 30 \frac{\text{mg}}{\text{kg}}$) and the cell kill rate was set at 0.00161 $\frac{\text{mL}}{\mu\text{g hr}}$. A change in cell-phase specificity does not alter the GM PD effect, so k_D remained at 0.00325 $\frac{\text{mL}}{\mu\text{g hr}}$.

Figure 12 shows the predicted PD fit using the SCM-M, GM (including drug effect), and actual data. The SCM-M was able to capture the tumor response profile and coincides with the Gompertz predictions, demonstrating similar behavior for short dosing periods. In addition, it is interesting to note that the SCM-G also fit this data. All three models display similar tumor volume responses for the dosing regimen and time periods in question, despite each having a different location for kill term effect.

Similar to the previous mismatch studies, the SCM-M was set as the "simulated mouse" and tested using either the mismatch case Gompertz model as the controller model initialized with equivalent input (MC-Mu) or the nominal case saturating rate cell-cycle model with M-phase kill (NC-M) as the controller model. To maintain a steady 100 mm^3 xenograft tumor burden in the SCM-M, a daily dose of 9.5 $\frac{\text{mg}}{\text{kg}}$ was necessary, corresponding to a 262 mm^3 tumor volume for the GM. Initialization employed the same steady state dose to enable variable manipulation over the entire dosing range. The two test cases comparing stepwise reduction in tumor volume and biweekly dosing updates were simulated to determine whether performance similarity between the NC-G and MC-Gu controllers was a result of a G-phase chemotherapeutic acting on a predominantly G-phase tumor.

The results of the four-stage reduction in tumor volume simulation are shown in Figure 13. The MC-Mu controller was unable to follow the desired trajectory for the entire simulation, never reaching a stable tumor volume within 1% of desired by the time of the next decrement. The total drug delivered by the MC-Mu was 5% less than the NC-M system. Furthermore, the GM-based controller was less aggressive, delivering less drug initially, but

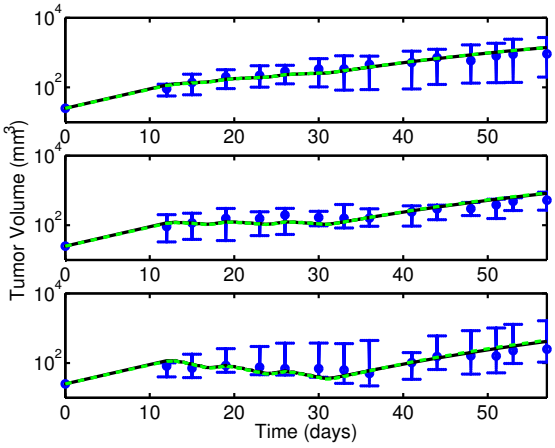

Fig. 12. Measured MCF-7 tumor xenograft data for tumor-bearing athymic mice (circles) vs. model predictions for the SCM-M (solid), and the GM (dashed) dosed orally at 7.5 (top), 15 (middle) or 30 mg/kg (bottom) TM per day. Error bars represent a 95% confidence interval.

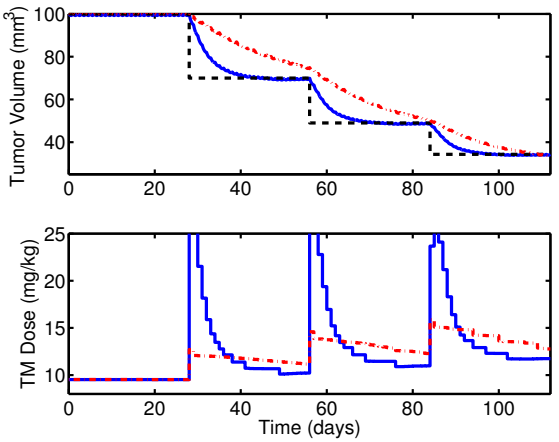

Fig. 13. Tumor volume (top), reference volume (dashed, top) and TM dose representation (bottom) as a function of time. Tuning parameters were chosen as m = 1 and p = 8 for both the nominal (NC-M, solid) and mismatch (MC-Mu, dash-dot) cases.

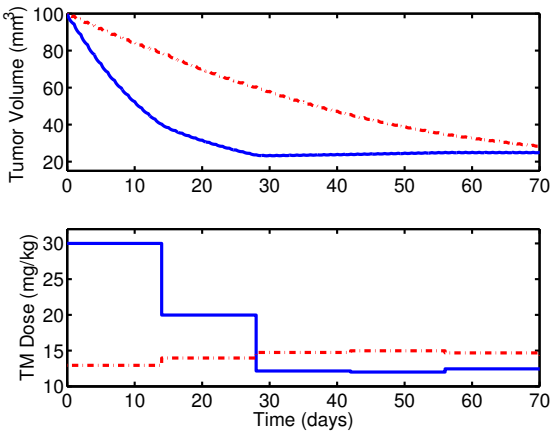

Fig. 14. Tumor volume (top) and TM dose representation (bottom) as a function of time. Tumor volumes are measured biweekly under NMPC with $m = 1$, $p = 21$ for the nominal (NC-M, solid) and mismatch (MC-Mu, dash-dot) cases. The tumor volume reference value is 25 mm^3.

maintaining an elevated dose level for an extended period of time. This significantly different dosing profile contributed to the MC-Mu system falling short of the desired trajectory by 1-5% at the end of each stage. A final point of concern is the trajectory taken by the MC-Mu controller following the step from 100 to 70 mm^3. The response was more sluggish, likely a result of the initial conditions for the model's operating state. While the NC-M maintains a steady tumor burden of 100 mm^3 at a dose of 9.5 $\frac{\text{mg}}{\text{kg}}$, the same dosing resulted in a GM predicted volume of 262 mm^3. At this operating state, small changes in dose were predicted to cause large alterations in the tumor volume, and the controller took a less aggressive approach toward the desired reference trajectory.

This point is further illustrated in Figure 14 where tumor dosing is updated biweekly. The NC-M controller rapidly drove the tumor volume toward the desired trajectory of 25 mm^3, settling to within 1% of the desired setpoint by 28 days. The MC-Mu controller, however, resulted in a trajectory that had not reached the reference criteria by 72 days. The dosing profile proves that the MC-Mu controller yielded a less aggressive response, a side effect of the large steady state tumor volume at the starting dose.

To improve controller performance, the GM was initialized with identical tumor volume (MC-My) to the "simulated mouse" (100 mm^3) instead of equivalent drug input (9.5 $\frac{\text{mg}}{\text{kg}}$). For this tumor burden, the GM required a steady state drug delivery of 12.0 $\frac{\text{mg}}{\text{kg}}$. Maintaining both dosing inputs within the constraints, $0 \leq \mathscr{U}(k|k) \leq 30\frac{\text{mg}}{\text{kg}}$, required redefining the input constraints as $2.5 \leq \mathscr{U}(k|k) \leq 27.5\frac{\text{mg}}{\text{kg}}$. The reduction in range for lower dosing levels did not significantly impact tumor treatment as the manipulated variable did not enter this range for all investigated simulations. Dose predictions within the excluded upper range, however, were implemented immediately following negative steps in the reference trajectory and contribute to the initial, rapid tumor size reduction.

Revisiting the constraint development, it was observed that doses within the range of 7.5 to $30\frac{\text{mg}}{\text{kg}}$ resulted in similar tumor-kill rates while k_D at doses of $60\frac{\text{mg}}{\text{kg}}$ were markedly reduced, possibly as a result of receptor saturation. The dose at which saturation begins (between $30 - 60\frac{\text{mg}}{\text{kg}}$) was not explicitly known. If one assumed that doses slightly above $30\frac{\text{mg}}{\text{kg}}$ would not achieve saturation, the following magnitude constraints can be enforced: $2.5 \leq \mathscr{U}(k|k) \leq 30\frac{\text{mg}}{\text{kg}}$. A performance comparison between the NC-M, MC-Mu, and GM controllers initialized at equivalent tumor volumes (MC-My), can be found in Figure 15. The NC-M response is identical to that for the first step in Figure 13 (analyzed above). In response to a decrease in desired tumor volume (100 $\rightarrow$ 70 mm^3), the MC-My controller was more aggressive than the MC-Mu controller. Both had trajectories which undershoot and eventually settle to within 1% of the desired tumor volume, however the MC-My controller reached the desired tumor volume faster and had the smaller $t_{99\%}$.

The stepwise tumor volume reduction and biweekly update test cases were simulated for the NC-M and the MC-My controllers; results are shown in Figures 16 and 17, respectively. The MC-My controller dosed more aggressively than the MC-Mu controller for the four-stage trajectory, and the MC-My system reached the desired reference on the same day as the NC-M system. Undershoot occurred for each step and settling to within 1% of the desired value was not achieved

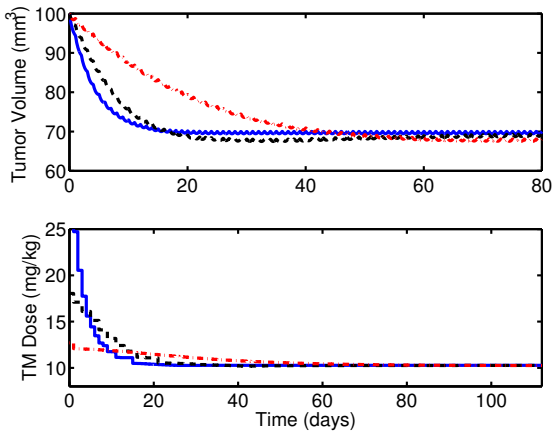

Fig. 15. Tumor volume (top) and TM dose representation (bottom) as a function of time. For tuning parameters of $m = 1$ and $p = 8$, the predicted trajectory is shown for the nominal (NC-M, solid) and the mismatch (MC-My, dashed; MC-Mu, dash-dot) cases. Reference tumor volume was 70 mm^3.

during any of the four-week stages. Similarly, a more aggressive trajectory was taken by the MC-My system in the biweekly update study. Undershoot resulted during weeks 3-4 with oscillations around the desired trajectory ceasing by week 16 (not shown). In both cases superior controller performance was achieved with the MC-My vs. the MC-Mu (results in Figures 13 and 14, provided that undershoot in tumor volume can be tolerated). These new controller settings were not able to outperform the NC-M, taking more time to settle in all studies. Furthermore, these results demonstrate the importance of incorporating cell-cycle information, especially if the fraction of the susceptible tumor population is small compared to the total tumor population (as is the case for an S- or M-phase targeted drug).

9. SUMMARY

A NMPC controller was designed to dose TM, a cycle-specific chemotherapeutic, to mice implanted with ER+ breast cancer xenografts. This controller is based on novel PK and PD models of TM dose and MCF-7 tumor growth, and the algorithm is ready for testing in a preclinical setting on mice. Adaptation to actual breast cancer patients would require TM PK and PD data from humans, but the model predictive control framework provides the groundwork for a patient-tailored dosing algorithm capable of constraining drug delivery within safety-induced bounds and responding to changes in patient response.

The closed loop system designed with the linear cell-cycle model in the controller was unable to track the four-stage trajectory for tumor volume reduction. Employing the less detailed nonlinear GM in the controller design resulted in similar trajectory tracking

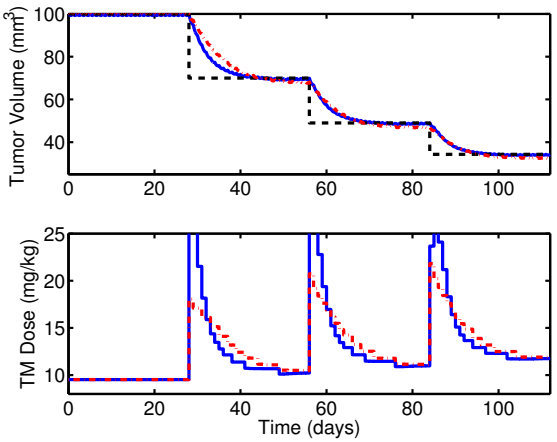

Fig. 16. Tumor volume (top) and TM dose representation (bottom) as a function of time. For tuning parameters of $m = 1$ and $p = 8$, the predicted trajectory is shown for the NC-M (solid) and MC-My (dash-dot) systems. Reference tumor volume decreased every 4 weeks, starting at 100 mm^3.

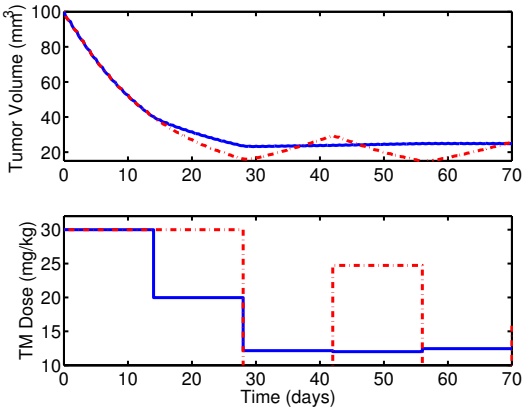

Fig. 17. Tumor volume (top) and TM dose representation (bottom) as a function of time. Tumor volumes are measured biweekly under NMPC with $m = 1$, $p = 21$ for the NC-M (solid) and the MC-My (dash-dot) cases. Reference tumor volume was 25 mm^3.

results when compared to controllers designed with the more complex SCM. Controller performance was dependent on the cycle phase of drug effect, with more significant performance deviation between the nominal and mismatch systems when the drug effect targeted a smaller portion of the the overall tumor population (M vs. G). Furthermore, given the rate at which tumor volume measurements are taken in the clinic, failure to track cell phase for cycle-specific chemotherapeutics can lead to gross misestimates in tumor volume reductions. Future foci include toxicity modeling/monitoring (*e.g.* white blood cell count) and development of a multi-rate NMPC algorithm with state estimation to allow toxicity- and efficacy-driven changes to the dosing profile in real-time.

10. ACKNOWLEDGMENTS

The authors would like to acknowledge funding in the form of a Whitaker Foundation Graduate Student Fellowship (JAF) and the Fulton C. Noss faculty fellowship (RSP). The animal studies from (Conley *et al.*, 1999) were funded by the NIH/NCI (N01-CM27752).

11. REFERENCES

Akaike, A. (1979). A Basian Extension of the Minimal AIC Procedures of Autoregressive Model Fitting. *Biometrika* **66**, 237.

Asachenkov, A., G. Marchuk, R. Mohler and S. Zuev (1994). *Disease Dynamics*. Birkhäuser. Boston.

Bajzer, Ž., M. Marušić and S. Vuk-Pavlović (1996). Conceptual frameworks for mathematical modeling of tumor growth dynamics. *Math. Comput. Model.* **23**(6), 31–46.

Conley, B. A., T. S. Ramsland, D. L. Sentz, S. Wu, D. M. Rosen, M. Wollman and J. L. Eiseman (1999). Antitumor activity, distribution, and metabolism of 13-*cis*-retinoic acid as a single agent or in combination with tamoxifen in established human MCF-7 xenografts in mice. *Cancer Chemother. Pharmacol.* **43**, 183–197.

D'Argenio, D. Z. and A. Schumitzky (1997). *ADAPT II Users Guide: Pharmacokinetic and Pharmacodynamic Systems Analysis Software*. Biomedical Simulations Resource, University of Southern California. Los Angeles, CA.

Ellis, M. J. and S. M. Swain (2001). Steroid hormone therapies for cancer. In: *Cancer Chemotherapy and Biotherapy: Principles and Practice* (B. A. Chabner and D. L. Longo, Eds.). 3rd ed.. pp. 103–13. Lippincott Williams and Wilkins.

Florian Jr., J. A., J. L. Eiseman and R. S. Parker (2003). Approximating cancer tumor growth dynamics using cell-cycle models in series. In: *AIChE Annual Meeting*. paper 439ab. San Francisco, CA.

Harrold, J. M., J. L. Eiseman, W. C. Zamboni and R. S. Parker (2003). A clinically relevant mixed integer approach to cancer chemotherapy treatment design. In: *AIChE Annual Meeting*. paper 478a. San Francisco, CA.

Kozusko, F., P. Chen, S. G. Grant, B. W. Day and J. C. Panetta (2001). A mathematical model of in vitro cancer cell growth and treatment with the antimitotic agent curacin A. *Mathimatical Biosciences* **170**, 1–16.

Ledzewicz, U. and H. Schättler (2002). Optimal bang-bang controls for a two-compartment model in cancer chemotherapy. *J. Optimization Theory Appl.* **114**(3), 609–637.

Lee, G. S., K. S. Ryu, S. P. Kim, S. E. Namkoong and K. T. Han (2002). Multiparametric flow cytometric analysis in a breast cancer cell line (MCF-7). *J. Obstet. Gynaecol. Res.* **28**(3), 141–8.

Lopes, N. M., E. G. Adams and B. K. Bhuyan (1993). Cell kill kinetics and cell cycle effects of taxol on human and hamster ovarian cell lines. *Cancer Chemoth. Pharm.* **32**(3), 235–242.

Martin, E. A., P. Carthew, I. N. White, R. T. Heydon, M. Gaskell, R. J. Mauthe, K. W. Turteltaub and L. L. Smith (1997). Invesitgation of the formation and accumulation of liver DNA adducts in mice chronically exposed to tamoxifen. *Carcinogenesis* **18**(11), 2209–15.

Martin, R. and K. L. Teo (1994). *Optimal Control of Drug Administration in Cancer Chemotherapy*. World Scientific. River Edge, NJ.

Martin, R. B. (1992). Optimal control drug scheduling of cancer chemotherapy. *Automatica* **28**, 1113–1123.

Morari, M. and E. Zafiriou (1989). *Robust Process Control*. Prentice-Hall, Englewood Cliffs, NJ.

Morari, M. and N. L. Ricker (1994). *Model Predictive Control Toolbox*. The MathWorks, Inc.. Natick, MA.

Norton, L. (1988). A Gompertzian model of human breast cancer growth. *Cancer Res.* **48**, 7067–7071.

Panetta, J. C. and J. Adam (1995). A mathematical model of cycle–specific chemotherapy. *Math. Comput. Model.* **22**(2), 67–82.

Riesberg, M., C. Kasper, K. F. Reardon and T. Scheper (2001). Flow cytometry in biotechnology. *Appl. Microbiol. Biotechnol.* **56**, 350–60.

Robinson, S. P., S. M. Langan-Fahey, A. J. Delinda and V. C. Jordan (1991). Metabolites, pharmacodynamics, and pharmacokinetics of tamoxifen in rats and mice compared to the breast cancer patient. *Drug Metabolism and Disposition* **19**(1), 36–43.

The American Cancer Society (2004). Cancer facts & figures: 2004. URL: http://www.cancer.org/downloads/STT/CAFF_finalPWSecured.pdf.